AIAA JOURNAL
Vol. 39, No. 4, April 2001

Nonlinear Supersonic Flutter of Circular Cylindrical Shells

Marco Amabili*
Università di Parma, I-43100 Parma, Italy
and
Francesco Pellicano†
Università di Modena e Reggio Emilia, I-41100 Modena, Italy

The aeroelastic stability of simply supported, circular cylindrical shells in supersonic flow is investigated. Nonlinearities caused by large-amplitude shell motion are considered by using the Donnell nonlinear shallow-shell theory, and the effect of viscous structural damping is taken into account. Two different in-plane constraints are applied to the shell edges: zero axial force and zero axial displacement; the other boundary conditions are those for simply supported shells. Linear piston theory is applied to describe the fluid–structure interaction by using two different formulations, taking into account or neglecting the curvature correction term. The system is discretized by Galerkin projections and is investigated by using a model involving seven degrees of freedom, allowing for traveling-wave flutter of the shell and shell axisymmetric contraction. Results show that the system loses stability by standing-wave flutter through supercritical bifurcation; however, traveling-wave flutter appears with a very small increment of the freestream static pressure that is used as the bifurcation parameter. A very good agreement between theoretical and existing experimental data has been found for flutter amplitudes. The influence of internal static pressure has also been studied.

Nomenclature

$A_{m,n}(t)$, $B_{m,n}(t)$	=	modal coordinates (time dependent)
a_∞	=	freestream speed of sound
c	=	damping parameter
D	=	flexural rigidity of the shell
E	=	Young's modulus
F	=	Airy stress function
h	=	shell thickness
L	=	shell length
M	=	Mach number
m	=	number of axial half-waves
N_x, N_θ, $N_{x,\theta}$	=	axial, circumferential, and shear forces per unit length
n	=	number of circumferential waves
p	=	radial aerodynamic pressure
p_m	=	pressure differential across the shell skin
p_∞	=	freestream static pressure
R	=	shell radius
t	=	time
u	=	axial shell displacement
v	=	circumferential shell displacement
w	=	radial shell displacement
x	=	longitudinal coordinate
γ	=	adiabatic exponent
ζ	=	modal damping coefficient
θ	=	angular coordinate
ρ	=	mass density of the shell

I. Introduction

THE aeroelastic stability of cylindrical shells in axial flow is of keen interest in the design of skin panels on aerospace vehicles, high-performance aircraft, and missiles. The first reported occurrence of flutter instability on these structures appears to have been on the V-2 rocket. The theories available for the stability of circular cylindrical shells in flow do not agree sufficiently well with the experimental results, as pointed out by Horn et al.,[1] and even today no satisfactory design criterion is available. In particular, for subsonic Mach numbers, highly divergent and catastrophic instabilities have been measured experimentally for clamped-clamped copper shells excited by a fully developed turbulent flow.[1] This kind of instability has recently been explained by Amabili et al. by using a nonlinear shell model and potential flow in cases of both internal[2] and external subsonic flow.[3] Numerical results are in agreement with experimental data for annular airflow.[4]

Many interesting studies have investigated the shell stability in supersonic flow, predicting flutter, by using a linear shell model; among others, Dowell,[5] Olson and Fung,[6,7] Barr and Stearman,[8] and Ganapathi et al.[9] However, experiments have indicated that the oscillation amplitude of flutter is of the same order of the shell thickness; therefore, a nonlinear shell theory must be used in order to predict accurately flutter amplitude.

Only a few researchers used a nonlinear shell model to investigate the aeroelastic stability of cylindrical shells in axial supersonic flow. Librescu[10,11] studied the stability of shallow panels and finite-length circular cylindrical shells by using the Donnell nonlinear shallow-shell theory and a simple mode expansion without considering the companion mode (a second standing-wave mode, the orientation of which is at $\pi/2n$ with respect to the original one, the so-called driven mode, n being the number of nodal diameters) and interaction with axisymmetric modes. As pointed out by several authors (see, e.g., Refs. 12–18), expansions neglecting axisymmetric modes are not able to capture the correct nonlinear behavior of circular shells and are only suitable for panels. The absence of the companion mode does not permit traveling-wave flutter. The theory developed by Librescu[10,11] is also suitable for composite shells, and nonlinear terms are included in the fluid pressure obtained by piston theory. No results on limit cycle amplitudes are given.

Olson and Fung[7] modeled simply supported shells by using a simplified form of the Donnell nonlinear shallow-shell theory and a simple two-mode expansion without considering the companion mode but including an axisymmetric term. In their study, the supersonic flow was modeled by using the linear piston theory. In subsequent studies, Evensen and Olson[12,13] also considered the companion mode, therefore using a four-degree-of-freedom mode expansion. This expansion allows the study of traveling-wave flutter, in which nodal lines are traveling circumferentially around the shell; this phenomenon is similar to traveling waves predicted and measured for large-amplitude forced vibrations of shells.[14–18] However, similarly to Evensen's[14] expansion for the flexural shell displacement, these expansions are not moment free at the ends of

Received 15 March 2000; revision received 27 June 2000; accepted for publication 30 June 2000.

*Associate Professor, Department of Industrial Engineering; marco@me.unipr.it.
†Assistant Professor, Department of Engineering Science.

the shell, as they should be for classical simply supported shells, and the homogeneous solution for the stress function is neglected. Evensen and Olson[12,13] investigated periodic solutions by using the harmonic balance method and solved the nonlinear algebraic equations only for some special cases. The results obtained are different, from the qualitative point of view, with respect to those of Olson and Fung[7]; this is due to the different order of the perturbation approach used. Olsson[19] added to the problem the effect of a particular temperature field on material properties by using a simple two-mode expansion.

A full literature review of works on the nonlinear dynamics of shells in vacuo and filled with or surrounded by quiescent fluid is given by Amabili et al.[17] and will not be repeated here. One important conclusion reached in that study, however, is the following. Because most analyses involve some kind of Galerkin-type expansion, the choice of appropriate comparison functions is always important, but in the case of nonlinear shell motions it is crucial, for the presence of opposite effects that are due to quadratic and cubic nonlinearities. A linear modal base is the simplest and best choice. Furthermore, in order to reduce the number of degrees of freedom, it is important to use only the most significant modes. Thus, in addition to representing both the regular or "driven" asymmetric modes and the "companion modes," it is also important to include axisymmetric modes. This is because it has been clearly established that, for nonlinear shell vibrations, the deformation of the shell involves a small but important axisymmetric contraction of the circumference. As a consequence of this effect, shell displacements inward are slightly larger than those outward. This is important in predicting the kind of softening behavior that has been observed in the experiments. Moreover, the interaction of the shell with a dense fluid reduces the frequencies of axisymmetric modes more than those of asymmetric modes, significantly increasing the nonlinearity of the structure.[17,18,20]

The nonlinear stability of simply supported, circular cylindrical shells in supersonic axial flow is reinvestigated in the present study by using an improved structural model. The present approach is based on the nonlinear shell model developed by Amabili et al.[2] to study stability of shells containing incompressible flow. Nonlinearities that are due to large-amplitude shell motion are considered by using the Donnell nonlinear shallow-shell theory, also taking into account the effect of viscous structural damping. Two different in-plane constraints are applied to the shell edges: zero axial force and zero axial displacement; the other boundary conditions are those for simply supported shells. The fluid–structure interaction is described by two different versions of the linear piston theory. Experimental observations cast doubt as to the validity of using linear piston theory to describe the unsteady pressure field over the shell because of the influence of the viscous boundary layer. However, for the configurations investigated in the present study related to experiments performed by Olson and Fung,[6,7] the pertinent streamwise wavelengths of interest are very large with respect to the boundary layer thickness, so the influence of the boundary layer is probably negligible. There is no contradiction in using a nonlinear theory to describe shell motion with a linear theory for the shell–flow interaction. In fact, a displacement of the order of the shell thickness introduces significant nonlinearities in the equations of motion; in contrast, a linear analysis of the aerodynamics is still appropriate for the small fluid perturbation velocities associated with such small shell deformations.

The system is discretized by Galerkin projection, leading to a seven-degree-of-freedom model, allowing for traveling-wave flutter and shell axisymmetric contraction. Numerical calculations have been performed for a copper circular shell, fabricated by electroplating and tested in the 8×7 ft supersonic wind tunnel at the NASA Ames Research Center.[6,7] Theoretical results for the two versions of the piston theory show that the system loses stability by standing-wave flutter through supercritical bifurcation; however, traveling-wave flutter appears with a very small increment of the freestream static pressure that is used as the bifurcation parameter. Theoretical results show flutter amplitudes in very good agreement with the NASA experimental results. The influence of internal static pressure has been studied.

II. Equation of Motion and Boundary Conditions

A cylindrical coordinate system (O; x, r, θ) is chosen, with the origin O placed at the center of one end of the shell. The displacements of points in the middle surface of the shell are denoted by u, v, and w, in the axial, circumferential, and radial directions, respectively. With the use of the Donnell nonlinear shallow-shell theory, the equation of motion for large-amplitude transverse vibrations of a very thin, circular cylindrical shell is given by[14,16]

$$D\nabla^4 w + ch\dot{w} + \rho h\ddot{w} = p - p_m + \frac{1}{R}\frac{\partial^2 F}{\partial x^2} + \frac{1}{R^2}\left(\frac{\partial^2 F}{\partial \theta^2}\frac{\partial^2 w}{\partial x^2} - 2\frac{\partial^2 F}{\partial x \partial \theta}\frac{\partial^2 w}{\partial x \partial \theta} + \frac{\partial^2 F}{\partial x^2}\frac{\partial^2 w}{\partial \theta^2}\right) \tag{1}$$

where $D = Eh^3/\ 12(1-\nu^2)]$ is the flexural rigidity, E is Young's modulus, ν is the Poisson ratio, h is the shell thickness, R is the mean shell radius, ρ is the mass density of the shell, c is the damping parameter, p is the radial aerodynamic pressure applied to the surface of the shell as a consequence of the external supersonic flow (positive inward), and p_m is the pressure differential across the shell skin (positive outward). The radial deflection w is positive inward; the overdot denotes a time derivative, and F is the in-plane Airy stress function. Here F is given by the following relation[14,16]:

$$\frac{1}{Eh}\nabla^4 F = -\frac{1}{R}\frac{\partial^2 w}{\partial x^2} + \frac{1}{R^2}\left[\left(\frac{\partial^2 w}{\partial x \partial \theta}\right)^2 - \frac{\partial^2 w}{\partial x^2}\frac{\partial^2 w}{\partial \theta^2}\right] \tag{2}$$

In Eqs. (1) and (2), the biharmonic operator is defined as $\nabla^4 = \partial^2/\partial x^2 + \partial^2/(R^2\partial\theta^2)]^2$. The Donnell nonlinear shallow-shell equations are accurate only for modes of high circumferential wave number n (n is the number of nodal diameters); specifically, $1/n^2 \ll 1$ must be satisfied, so that $n \geq 5$ is required in order to have fairly good accuracy. Donnell nonlinear shallow-shell equations are obtained by neglecting the in-plane inertia, transverse shear deformation, and rotary inertia, giving accurate results only for very thin shells; that is, $h \ll R$. In-plane displacements are infinitesimal, that is, $|u| \ll h$, $|v| \ll h$, whereas w is of the same order of the shell thickness, $|w| = \mathrm{O}(h)$. The predominant nonlinear terms are retained but other secondary effects, such as the nonlinearities in curvature strains, have been neglected; in particular, the curvature changes are expressed by linear functions of w only.

The forces per unit length in the axial and circumferential directions, as well as the shear force, are given by[21,22]

$$N_x = \frac{1}{R^2}\frac{\partial^2 F}{\partial \theta^2}, \qquad N_\theta = \frac{\partial^2 F}{\partial x^2}, \qquad N_{x\theta} = -\frac{1}{R}\frac{\partial^2 F}{\partial x \partial \theta} \tag{3}$$

The strain-displacement relations are[21,22]

$$(1-\nu^2)\frac{N_x}{Eh} = -\frac{\nu w}{R} + \frac{1}{2}\left(\frac{\partial w}{\partial x}\right)^2 + \frac{\nu}{2}\left(\frac{\partial w}{R\partial\theta}\right)^2 + \frac{\partial u}{\partial x} + \frac{\nu}{R}\frac{\partial v}{\partial \theta} \tag{4}$$

$$(1-\nu^2)\frac{N_\theta}{Eh} = -\frac{w}{R} + \frac{\nu}{2}\left(\frac{\partial w}{\partial x}\right)^2 + \frac{1}{2}\left(\frac{\partial w}{R\partial\theta}\right)^2 + \nu\frac{\partial u}{\partial x} + \frac{1}{R}\frac{\partial v}{\partial \theta} \tag{5}$$

$$(1-\nu^2)\frac{N_{x\theta}}{Eh} = 2(1-\nu)\left[\frac{1}{R}\frac{\partial w}{\partial x}\frac{\partial w}{\partial \theta} + \frac{1}{R}\frac{\partial u}{\partial \theta} + \frac{\partial v}{\partial x}\right] \tag{6}$$

In this study, attention is focused on both 1) a finite, simply supported, circumferentially closed circular cylindrical shell of length L, and 2) an infinitely long shell, periodically supported. In the latter case, the portion of the shell considered lies between two supports, L apart, while the effect of the part of the shell beyond is only considered as a constraint.

In both cases the following boundary conditions must be satisfied:

$$w = 0, \qquad M_x = -D\left[\left(\frac{\partial^2 w}{\partial x^2}\right) + \nu\left(\frac{\partial^2 w}{R^2\,\partial\theta^2}\right)\right] = 0 \qquad \text{at} \quad x = 0, L \tag{7}$$

where M_x is the bending moment per unit length. The other boundary conditions differ for the simply supported shell of finite length (case 1) and for the infinitely long, periodically supported shell with restrained axial displacement at the supports (case 2). They are as follows.

Case 1:

$$N_x = 0 \quad \text{at} \quad x = 0, L, \qquad v = 0 \quad \text{at} \quad x = 0, L \tag{8a}$$

Case 2:

$$u = 0 \quad \text{at} \quad x = 0, L, \qquad v = 0 \quad \text{at} \quad x = 0, L \tag{8b}$$

moreover, u, v, and w must be continuous in θ. Case 1 corresponds to the classical simply supported shell. Case 2 corresponds to antisymmetric modes (lower modes) with respect to each support; the conditions imposed in case 2 are well justified by the reciprocal constraint between the part of the shell under consideration and extensions thereof outside $(0, L)$. Case 2 also approximates a shell with rings at the ends. By use of the present formulation, it is also possible to study a shell subjected to axial prestress, that is, $N_x = \tilde{N}_x$ at $x = 0, L$.

The flexural deformation w is expanded by using the linear shell eigenmodes for zero flow as the base; in particular, the flexural response having n nodal diameters and m longitudinal half-waves can be written as follows[2]:

$$w(x, \theta, t) = \sum_{m=1}^{2} A_{m,n}(t)\cos(n\theta) + B_{m,n}(t)\sin(n\theta)]\sin(\lambda_m x) + \sum_{m=1}^{3} A_{(2m-1),0}(t)\sin\left(\lambda_{(2m-1)}x\right) \tag{9}$$

where $\lambda_m = m\pi/L$ and t is the time; $A_{m,n}(t)$, $B_{m,n}(t)$, and $A_{m,0}(t)$ are the modal coordinates that are unknown functions of t. Equation (9) was obtained by supposing that the nonlinear interaction among "linear modes" of the chosen base involves only the asymmetric modes ($n > 0$) having a given n value, and axisymmetric modes ($n = 0$) with an odd m value. Therefore, the nonlinear interaction with asymmetric modes of different n is neglected. For symmetry reason, only interaction with modes having $N \times n$ circumferential waves, where N is an integer, should be considered; however, the contribution of modes with $N > 1$ has been found to be negligible for large-amplitude vibrations of shells.[23] Axisymmetric modes having an even m value can be eliminated in the expansion; they do not contribute to the shell contraction and therefore, from mechanical considerations, their contribution to the shell dynamics is marginal. Axisymmetric modes play an important role in nonlinear oscillations, as pointed out in past studies,[14,17,18] and the interaction between asymmetric modes with the same n is fundamental in the investigation of shell stability in the case of supersonic flow. This is the reason why they are included in the present model. In particular, couple of asymmetric modes (driven and companion modes) having up to two axial half-waves, according to the two-mode linear piston theory[7] used to evaluate the fluid pressure on the shell, and axisymmetric modes having up to five axial half-waves (only odd terms) are retained, giving a seven-degree-of-freedom model.

III. Traveling-Wave Flutter

The presence of the companion mode in the periodic response of the shell leads to the appearance of traveling-wave flutter. The flexural mode shapes are represented by Eq. (9). Supposing harmonic flutter, it is possible to write $A_{1,n}(t) = \tilde{A}_{1,n}\cos(\omega t + \vartheta_1)$, $B_{1,n}(t) = \tilde{B}_{1,n}\cos(\omega t + \vartheta_2)$, $A_{2,n}(t) = \tilde{A}_{2,n}\cos(\omega t + \vartheta_3)$, and $B_{2,n}(t) = \tilde{B}_{2,n}\cos(\omega t + \vartheta_4)$. Thus Eq. (9) can be rearranged as

$$\begin{aligned} w = {} & \{\tilde{A}_{1,n}\cos(\omega t + \vartheta_1) + \tilde{B}_{1,n}\sin(\omega t + \vartheta_2)]\cos(n\theta) \\ & + \tilde{B}_{1,n}\sin(n\theta - \omega t - \vartheta_2)\}\sin(\pi x/L) \\ & + \{\tilde{A}_{2,n}\cos(\omega t + \vartheta_3) + \tilde{B}_{2,n}\sin(\omega t + \vartheta_4)]\cos(n\theta) \\ & + \tilde{B}_{2,n}\sin(n\theta - \omega t - \vartheta_4)\}\sin(2\pi x/L) + \mathcal{O}(\varepsilon^2) \end{aligned} \tag{10}$$

where ϑ_1, ϑ_2, ϑ_3, and ϑ_4 are the phase constants in the solution, ω is the radian flutter frequency, and ε is a small quantity. We denote by $\mathcal{O}(\varepsilon^2)$ small terms of higher order in the response of the shell. In Eq. (10), axisymmetric modes appear in higher-order terms as a consequence that they are small in amplitude.] Equation (10) gives two traveling waves of amplitude $\tilde{B}_{1,n}$ and $\tilde{B}_{2,n}$, radian frequency of rotation around the shell $\omega_T = \omega/n$, and two standing waves of radian frequency ω. The resulting standing wave with $m = 1$ is given by the sum of two standing waves, one of amplitude $\tilde{A}_{1,n}$ and the second of amplitude $\tilde{B}_{1,n}$, having the same radian frequency ω and the same shape, but having a phase difference of $\vartheta_2 - \vartheta_1 + \pi/2$ (similarly for $m = 2$). When $\vartheta_2 - \vartheta_1 \cong \pi/2$ and $\tilde{A}_{1,n} = \tilde{B}_{1,n}$, the amplitude of the resulting standing wave is zero and only a traveling-wave flutter appears for mode $m = 1$; when in addition $\vartheta_4 - \vartheta_3 \cong \pi/2$ and $\tilde{A}_{2,n} = \tilde{B}_{2,n}$, again only a traveling-wave flutter appears for all modes.

In general, the existence of driven, variable $A_{m,n}(t)$, and companion, variable $B_{m,n}(t)$, modes leads to the appearance of a circumferentially traveling wave and a standing wave; this phenomenon is related to the axial symmetry of the system. The traveling-wave flutter represents a fundamental difference vis-à-vis the linear approach to shell flutter.

IV. Piston Theory

The fluid–structure interaction is described by the linear piston theory. Higher-order piston theory[10] can be also applied to the present model but is left to future studies. As discussed in the Introduction, for the configurations investigated in the present study related to experiments performed by Olson and Fung,[6,7] the pertinent streamwise wavelengths of interest are very large with respect to the boundary layer thickness, so that the influence of the boundary layer is probably negligible.[7] The radial aerodynamic pressure p applied to the surface of the shell as a consequence of the external supersonic flow is approximated by a first-order piston theory[8]:

$$p = -\frac{\gamma p_\infty M^2}{(M^2-1)^{\frac{1}{2}}}\left\{\frac{\partial w}{\partial x} + \frac{1}{Ma_\infty}\left[\frac{M^2-2}{M^2-1}\right]\frac{\partial w}{\partial t} - \frac{w}{2(M^2-1)^{\frac{1}{2}}R}\right\} \tag{11}$$

where γ is the adiabatic exponent, p_∞ is the freestream static pressure, M is the Mach number, and a_∞ is the freestream speed of sound. In Eq. (11) the last term is the curvature correction term and is neglected in some studies of shell stability based on the piston theory.

A slightly different version of Eq. (11), based on a less accurate linearized potential flow expression and neglecting the curvature correction term, has been largely used in the past[7,12,13]:

$$p = -\gamma p_\infty\left\{M\frac{\partial w}{\partial x} + \frac{1}{a_\infty}\frac{\partial w}{\partial t}\right\} \tag{12}$$

Both Eqs. (11) and (12) are used and compared in the present study.

V. Airy Stress Function and Solution

The expansion used for the transverse displacement w satisfies identically the boundary conditions given by Eqs. (7); moreover, it satisfies exactly the continuity of circumferential displacement,

$$\int_0^{2\pi} \frac{\partial v}{\partial \theta}\,\mathrm{d}\theta = 0 \tag{13}$$

as shown by Amabili et al.[2] The boundary conditions for either of the in-plane displacements, Eqs. (8), give very complex expressions when transformed into equations involving w. Therefore they are modified into simpler integral expressions that satisfy Eqs. (8) on the average.[21] Specifically, the following conditions are imposed.

Case 1:

$$\int_0^{2\pi} N_x R\,\mathrm{d}\theta = 0, \qquad \text{at} \qquad x = 0, L \tag{14a}$$

Case 2:

$$\int_0^{2\pi}\int_0^{L}\frac{\partial u}{\partial x}\,\mathrm{d}x\,R\,\mathrm{d}\theta=\int_0^{2\pi}[u(L,\theta)-u(0,\theta)]R\,\mathrm{d}\theta=0 \qquad (14b)$$

For both cases:

$$\int_0^{2\pi}\int_0^{L}N_{x\theta}\,\mathrm{d}x\,R\,\mathrm{d}\theta=0 \qquad (15)$$

Equation (14a) ensures a zero axial force N_x on the average at $x=0, L$, whereas Eq. (14b) states that the axial displacement u is zero on the average at $x=0, L$. Equation (15) is satisfied when $v=0$ on the average at $x=0, L$ and u is continuous in θ on the average. Substitution of Eqs. (8) by Eqs. (14) and (15) simplifies computations, although it introduces an approximation (it can be proved that the boundary conditions are exactly satisfied at n discrete points, where n is the number of circumferential waves).

When the expansion of w, Eq. (9), is substituted in the right-hand side of Eq. (2), a partial differential equation for the stress function F is obtained, the solution of which may be written as

$$F=F_h+F_p \qquad (16)$$

where F_h is the homogeneous and F_p is the particular solution. The particular solution is given by

$$F_p=\sum_{m=0}^{M}\sum_{n=0}^{N}\{F_{1mn}\cos(n\theta)+F_{2mn}\sin(n\theta)]\sin(\lambda_m x)$$
$$+F_{3mn}\cos(n\theta)+F_{4mn}\sin(n\theta)]\cos(\lambda_m x)\} \qquad (17a)$$

where the functions of time F_{jmn}, $j=1,\ldots,4$, are given in Amabili et al.[2] The homogeneous solution may be assumed to have the form[2,17]

$$F_h=\frac{1}{2}\bar{N}_x R^2\theta^2+\frac{1}{2}x^2\left\{\bar{N}_\theta-\frac{1}{2\pi RL}\int_0^{L}\int_0^{2\pi}\left[\frac{\partial^2 F_p}{\partial x^2}\right]R\,\mathrm{d}\theta\,\mathrm{d}x\right\}$$
$$-\bar{N}_{x\theta}xR\theta \qquad (17b)$$

where $\bar{N}_x$, $\bar{N}_\theta$, and $\bar{N}_{x\theta}$ are the average in-plane force (per unit length) resultants, as a consequence of the in-plane constraints on the average, defined as

$$\bar{N}_{\#}=\frac{1}{2\pi L}\int_0^{2\pi}\int_0^{L}N_{\#}\,\mathrm{d}x\,\mathrm{d}\theta \qquad (18)$$

where the symbol # must be replaced by x, θ, and $x\theta$. Equation (17b) is chosen in order to satisfy the boundary conditions imposed. Moreover, it satisfies Eqs. (3) on the average as a consequence of 1) the contribution of F_p to $\bar{N}_\theta$ being

$$(2\pi RL)^{-1}\int_0^{L}\int_0^{2\pi}\left[\frac{\partial^2 F_p}{\partial x^2}\right]R\,\mathrm{d}\theta\,\mathrm{d}x$$

and 2) contributions of F_p to $\bar{N}_x$ and $\bar{N}_{x\theta}$ being zero. Boundary conditions (14) and (15) allow us to express the in-plane restraint stresses $\bar{N}_x$, $\bar{N}_\theta$, and $\bar{N}_{x\theta}$, see Eqs. (4–6), in terms of w and its derivatives.

By use of the Galerkin method, seven second-order ordinary, coupled nonlinear differential equations are obtained for the variables $A_{1,n}(t)$, $B_{1,n}(t)$, $A_{2,n}(t)$, $B_{2,n}(t)$, $A_{1,0}(t)$, $A_{3,0}(t)$, and $A_{5,0}(t)$, by successively weighing the single original equation with the functions that describe the shape of the seven modes retained in Eq. (9). These equations contain quadratic and cubic nonlinear terms. The Galerkin projection of the equation of motion (1) has been performed by using Mathematica computer software.[24]

VI. Effect of Internal Pressure

The effect of the pressure differential across the shell skin p_m can be evaluated by the solution of the equations of motion obtained by Galerkin projection. However, it is also possible to introduce a modified expression of the equation of motion (1) to take this effect into account immediately. This expression is an approximation of Eq. (1) based on the equilibrium for incremental deformations[25] and has been used by Olson and Fung[7] and by Evensen and Olson[12,13]:

$$D\nabla^4 w+ch\dot{w}+\rho h\ddot{w}=p+\bar{N}_x\frac{\partial^2 w}{\partial x^2}+\frac{\bar{N}_\theta}{R^2}\frac{\partial^2 w}{\partial\theta^2}+\frac{1}{R}\frac{\partial^2 F}{\partial x^2}$$
$$+\frac{1}{R^2}\left(\frac{\partial^2 F}{\partial\theta^2}\frac{\partial^2 w}{\partial x^2}-2\frac{\partial^2 F}{\partial x\partial\theta}\frac{\partial^2 w}{\partial x\partial\theta}+\frac{\partial^2 F}{\partial x^2}\frac{\partial^2 w}{\partial\theta^2}\right) \qquad (19)$$

where $\bar{N}_x$ and $\bar{N}_\theta$ are the membrane stress resultants. In particular,

$$\bar{N}_x=P_x/(2\pi R), \qquad \bar{N}_\theta=Rp_m \qquad (20)$$

and P_x is the total axial traction load applied to the shell and is always zero in the present study; P_x different from zero could be a result of external loads and internal pressure acting on the shell caps. The numerical results for pressurized shells has been obtained by using this approach.

VII. Numerical Results

Numerical results were obtained for a case already theoretically and experimentally studied by Olson and Fung[6,7] and by Evensen and Olson.[12,13] The case had the following characteristics: $R=0.2032$ m, $L=0.39116$ m, $R/h=2000$, $E=110.32\times10^9$ Pa, $\rho=8905.37$ kg/m^3, $\nu=0.35$, $\gamma=1.4$, $a_\infty=213.36$ m/s, $M=3$, and $p_m=3447.5$ N/m^2; the freestream stagnation temperature was 48.9°C. The test shell is extremely thin, fabricated with copper by electroplating, and tested in the 8×7 ft supersonic wind tunnel at the NASA Ames Research Center. The pertinent streamwise wavelengths of interest were measured to be very large with respect to the boundary layer thickness (see Fig. 5 in Ref. 6), so the influence of the boundary layer is probably negligible. These data will be used in all the following calculations, if not otherwise specified.

A. Linear Results

Results in this section have been obtained by using the linear part of Eqs. (2) and (19). Eigenvalues associated with the first and second longitudinal modes with 23 circumferential waves and damping coefficient $\zeta=0.0005$ are given in Fig. 1 vs the value of the freestream static pressure p_∞ by evaluating the aerodynamic pressure with

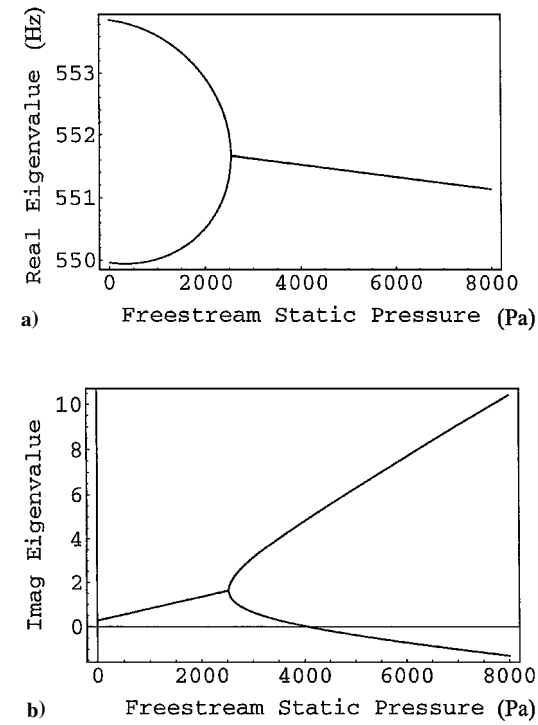

Fig. 1 a) Real part and b) imaginary part of the eigenvalues of the system vs the freestream static pressure p_∞ ; aerodynamic pressure evaluated with Eq. (11).

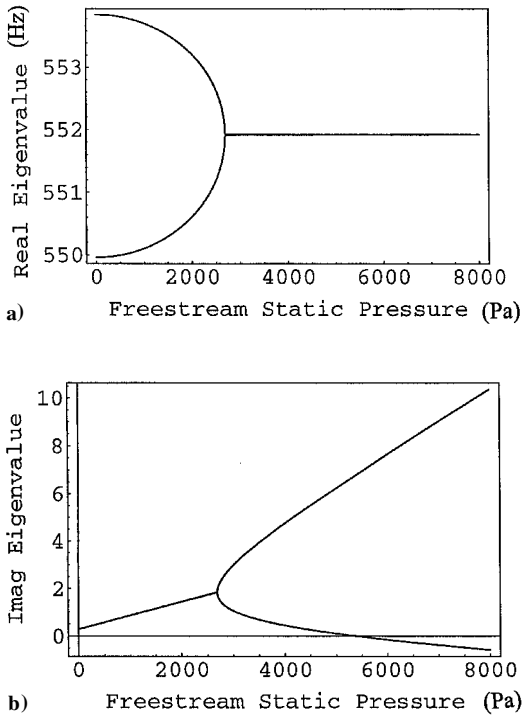

Fig. 2 a) Real part and b) imaginary part of the eigenvalues of the system vs the freestream static pressure p_∞ ; aerodynamic pressure evaluated with Eq. (12).

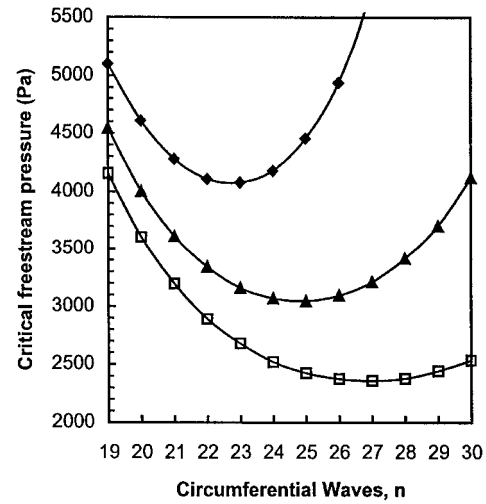

Fig. 3 Critical freestream static pressure obtained from the linearized equations vs the number n of circumferential waves: □, $p_m = 0$; ▲, $p_m = 1700$ Pa; and ♦, $p_m = 3447.5$ Pa.

Eq. (11). The real part of the eigenvalues gives the oscillation frequency, and the imaginary part is the exponent of the exponential function, giving damping for positive values and instability for negative values. Flutter starts where the imaginary part crosses the zero value, in this case for $p_\infty = 4077$ Pa; this value gives the critical freestream static pressure. In Fig. 1a the lower and higher of the two branches give the oscillation frequencies of the first and second modes (with $n = 23$), respectively. When they coalesce, a single mode is obtained and its oscillation frequency slowly decreases with p_∞ as a consequence that the stiffness of the system is reduced with an increase of p_∞ by the curvature correction term in Eq. (11). This mode originates flutter when the imaginary part of the eigenvalue becomes negative.

The same problem, studied by using the less accurate Eq. (12) instead of Eq. (11), gives the result shown in Fig. 2. The critical freestream static pressure is $p_\infty = 5373$ Pa; this value is reduced to $p_\infty = 4435$ Pa when no structural damping is considered and coincides with the value obtained by Evensen and Olson.[12,13] In Fig. 2a the flutter frequency is constant with an increase of p_∞. An important difference of ~30% is obtained in the present case between Eqs. (11) and (12).

The critical freestream static pressure is reported in Fig. 3 for different numbers of circumferential waves and for three values of pressure differential across the shell skin, that is, $p_m = 0$, 1700, and 3447.5 Pa. Data have been computed by using Eq. (11). The curve obtained for $p_m = 3447.5$ Pa shows that the value of n associated with the lowest critical freestream static pressure is $n = 23$, that is, the value used in Figs. 1 and 2. This value of n is augmented when p_m is decreased; moreover, internal pressure has a stabilizing effect on the system. All these results are in agreement with previous studies.[6–9]

B. Nonlinear Results

Solutions of the nonlinear equations of motion have been obtained numerically by using Auto software[26] for continuation of the solution and bifurcation of ordinary differential equations, based on a collocation method, and direct integration of the equations of motion. The Auto software is not able to detect surfaces coming out from a bifurcation point, but it can detect branches. As a consequence that, for the axisymmetry, the system does not possess a preferential angular coordinate θ to locate the deformation, in the present case surfaces come out from bifurcation points. In order to use Auto, a bifurcation analysis was performed by introducing a small perturbation to the linear part of the system. This approach is analogous to having a very small difference in the stiffness of the system for $\theta = 0, \pi/(2n)$, for example as a result of a small asymmetry in the shell. This imperfection allows normal bifurcation analysis, as line branches now emerge from bifurcation points instead of surfaces. A perturbation of 0.2% to the linear frequencies of companion modes has been used in the present case, so that differences with respect to the actual systems are almost negligible. Direct integration of the equations of motion by using an adaptive step-size fourth- to fifth-order Runge–Kutta method has also been performed to check the results and obtain the time behavior.

The bifurcation curves for all seven generalized coordinates vs the freestream static pressure are shown in Fig. 4 for the aerodynamic pressure given by Eq. (11), $n = 23$ and damping coefficient $\zeta = 0.0005$. These curves correspond to flutter amplitudes of the system (excluding branch 1 that is relative to equilibrium position). Results show that the system loses stability for $p_\infty = 4077$ Pa, that is, at the critical freestream static pressure obtained in Sec. VII.A by linear analysis. The solution can be imagined to evolve in three-dimensional plots of the pair of variables $\{A_{1,n}, B_{1,n}\}$ or $\{A_{2,n}, B_{2,n}\}$, relative to the first (or second) longitudinal mode, vs the freestream static pressure. Thus, a section of these three-dimensional plots gives the two-dimensional plots shown in Fig. 2. In Fig. 4, branch 1 corresponds to the trivial undeformed configuration that loses stability for $p_\infty = 4077$ Pa; at this value branch 2 arises through supercritical bifurcation. Branch 2 corresponds to standing-wave flutter, involving the first and second longitudinal mode with the same angular orientation. Actually, branch 3 also corresponds to this standing-wave flutter, with the same configuration of branch 2 but with an angular rotation of $\pi/(2n)$; in fact branches 2 and 3 are two-dimensional sections of the three-dimensional plots of the pair of variables $\{A_{1,n}, B_{1,n}\}$ or $\{A_{2,n}, B_{2,n}\}$ vs p_∞; these three-dimensional plots are surfaces of rotation around the p_∞ axis for the axisymmetry of the system. Here a small difference in the two-dimensional sections is observed as a consequence of the small perturbations introduced.

The standing-wave flutter loses stability very soon through bifurcation originating from branch 4. This branch 4 represents a traveling-wave flutter, as can be shown by observing the time traces of the system obtained by direct integration of the equations of motion for $p_\infty = 4500$ Pa, reported in Fig. 5. It can be observed that $\vartheta_2 - \vartheta_1 = \pi/2$, $\tilde{A}_{1,n} = \tilde{B}_{1,n}$, $\vartheta_4 - \vartheta_3 \cong \pi/2$, and $\tilde{A}_{2,n} = \tilde{B}_{2,n}$, giving pure traveling-wave flutter, as discussed in Sec. III. It is to be noted that, excluding a very small range of p_∞ after the onset of

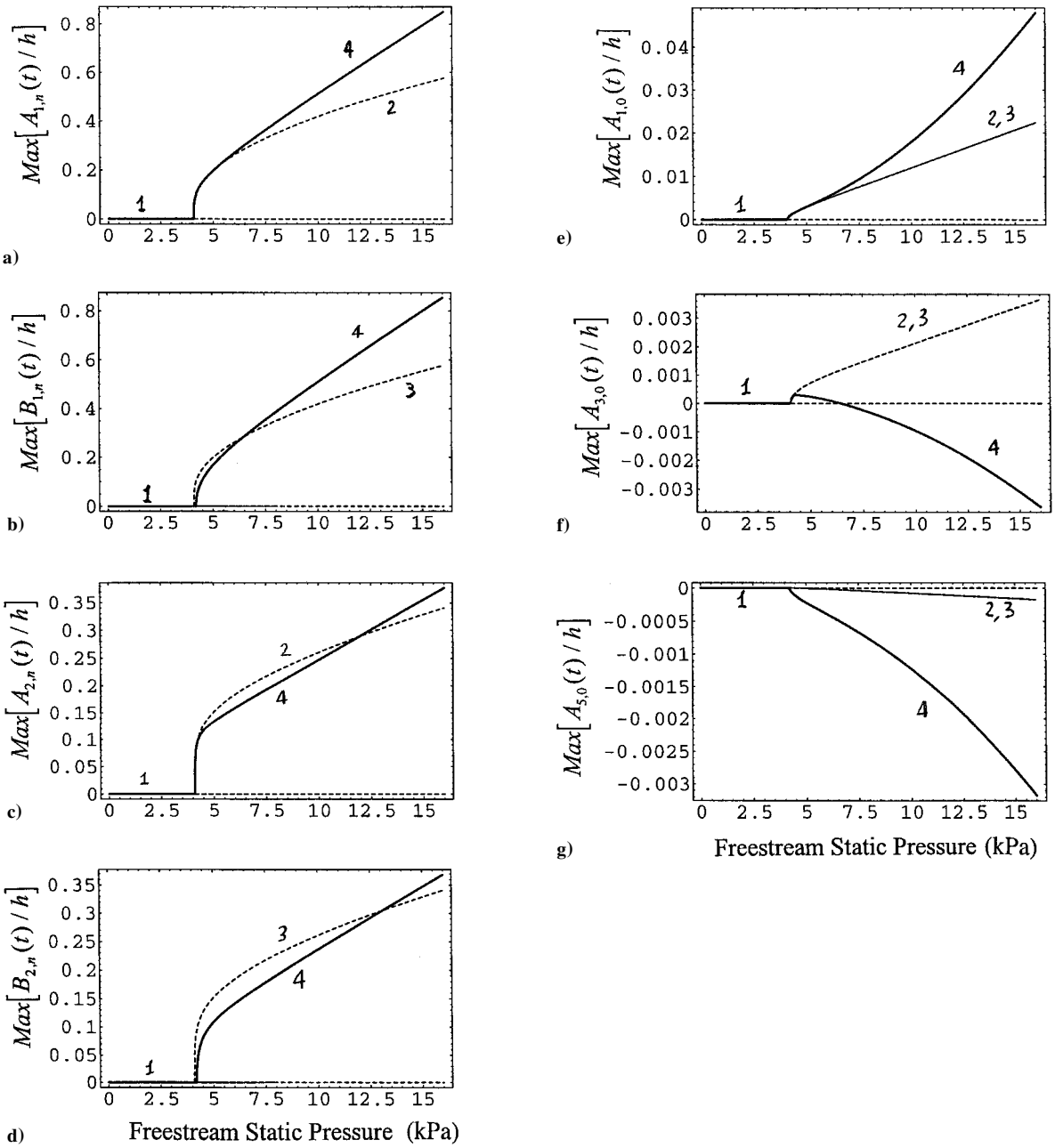

Fig. 4 Amplitude of oscillatory solutions vs the freestream static pressure: maximum amplitude of the first longitudinal mode a) $A_{1,n}(t)/h$ and b) $B_{1,n}(t)/h$; maximum amplitude of the second longitudinal mode c) $A_{2,n}(t)/h$ and d) $B_{2,n}(t)/h$; and maximum amplitude of the e) first, $A_{1,0}(t)/h$, f) third, $A_{3,0}(t)/h$, and g) fifth, $A_{5,0}(t)/h$, axisymmetric modes. Solid and dotted curves denote stable and unstable branches, respectively.

instability, all the stable flutter is a traveling wave around the circumference, as observed in the experiments by Olson and Fung[6] and predicted by Evensen and Olson.[12,13] The flutter amplitudes obtained in Fig. 4 are in excellent agreement with experimental results described by Olson and Fung in Ref. 6 for the same case. In particular, a maximum flutter amplitude of $\sim 0.5h_{\text{rms}}$ is reported for the studied case in Fig. 8 of Ref. 6, corresponding to $\sim 0.7h$ supposing sinusoidal oscillations.

Figure 6 shows the results obtained by direct integration of the equations of motion without perturbation of linear frequencies, slowly increasing the freestream static pressure. The system behavior is recorded after 2000 periods; to eliminate the transitory effect, the pressure is increased (or decreased) by 6 Pa for each step and a perturbation is given to the system at any step. Figure 6 describes the same flutter behavior obtained in Fig. 4 by using the Auto software, mainly confirming the previous results. Two small differences are found in the pressure range around the onset of flutter, $p_\infty = 4077$ Pa, and may be attributed to the frequency perturbation introduced in the system studied in Fig. 4. In particular, Figs. 6a and 6b are obtained by increasing the freestream static pressure and Figs. 6c and 6d by decreasing this pressure. All of the results show traveling-wave solutions; therefore, standing-wave flutter is stable only when the shell is not perfectly axisymmetric. Moreover, in Figs. 6a and 6b, a branch of small amplitudes is clearly shown that soon loses stability; the basin of attraction of this solution is quite small and in Figs. 6c and 6d, obtained decreasing the freestream static pressure, the main branch (branch 4 in Fig. 4) is followed.

The oscillation amplitude is reported in Fig. 7 vs the nondimensional flutter frequency for all the branches detected in Fig. 4. It is interesting to observe that a slightly softening behavior is obtained for the traveling-wave flutter, branch 4; however, this is due to the curvature-correctionterm in Eq. (11). The mode shape of flutter is given in Fig. 8 for $p_\infty = 4500$ Pa and shows a twist of the shell and a larger movement on the downstream part of the shell.

To compare the present results with those obtained by Evensen and Olson,[12,13] the simplified Eq. (12) has been also used to evaluate

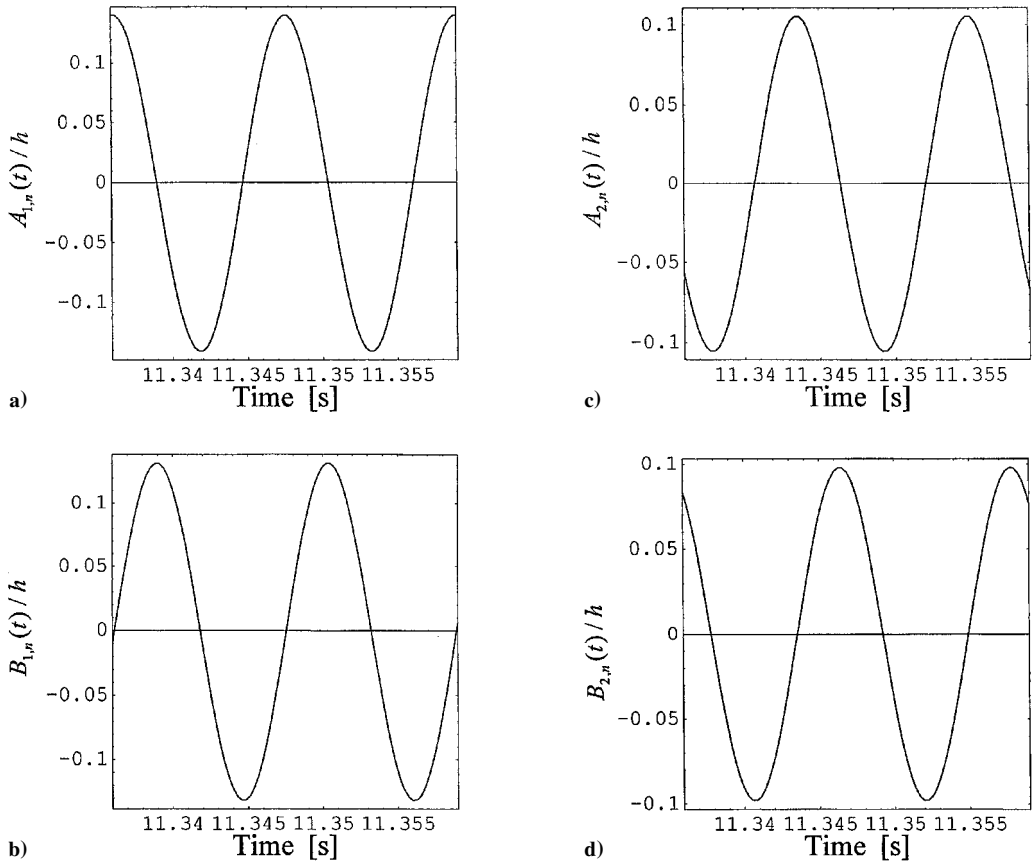

Fig. 5 Time traces of the system for $p_\infty = 4500$ Pa: amplitude of the first longitudinal mode a) $A_{1,n}(t)/h$ and b) $B_{1,n}(t)/h$; amplitude of the second longitudinal mode c) $A_{2,n}(t)/h$ and d) $B_{2,n}(t)/h$.

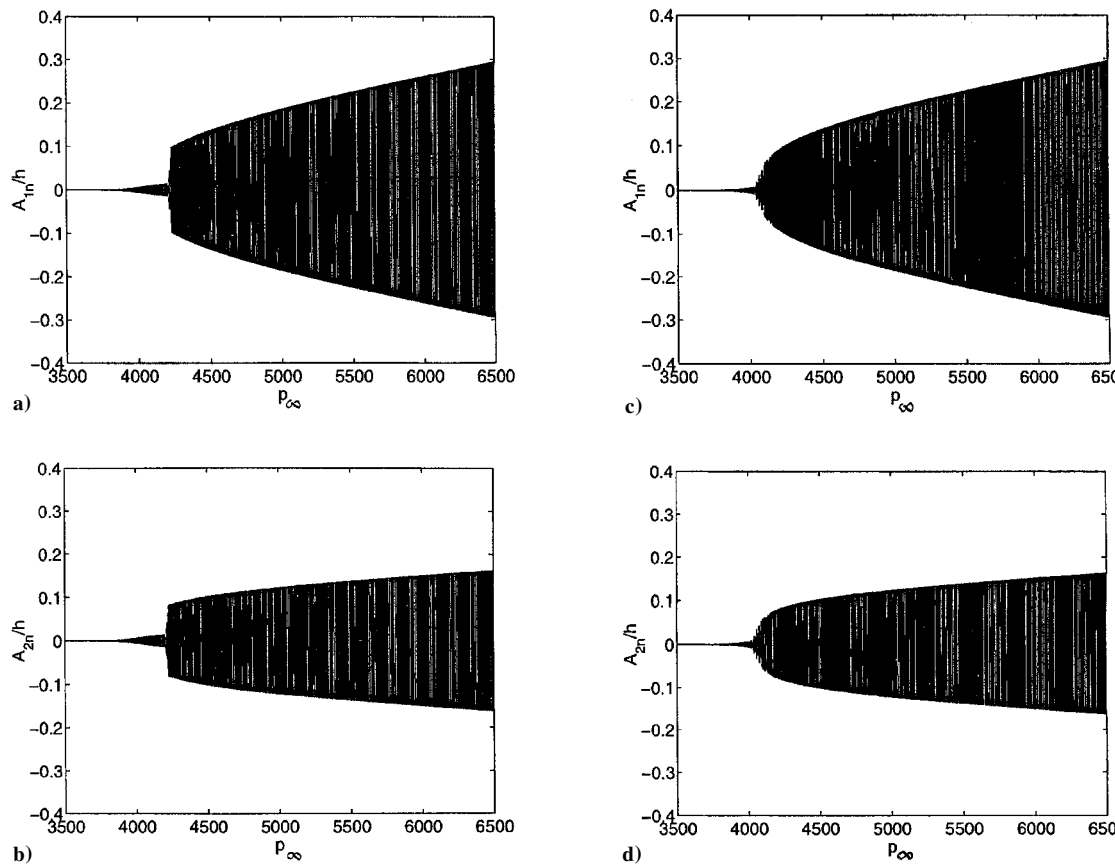

Fig. 6 Amplitude of oscillatory solutions vs the freestream static pressure (results are by direct integration of the equations of motion): a) $A_{1,n}(t)/h$ and b) $A_{2,n}(t)/h$ increasing the pressure; c) $A_{1,n}(t)/h$ and d) $A_{2,n}(t)/h$ decreasing the pressure.

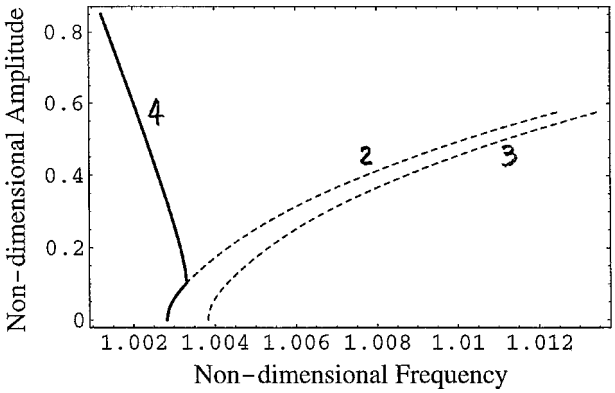

Fig. 7 Nondimensional flutter amplitude (maximum amplitude of the first longitudinal mode/h) vs nondimensional flutter frequency (flutter frequency/initial flutter frequency). Curve denotation is given in Fig. 4.

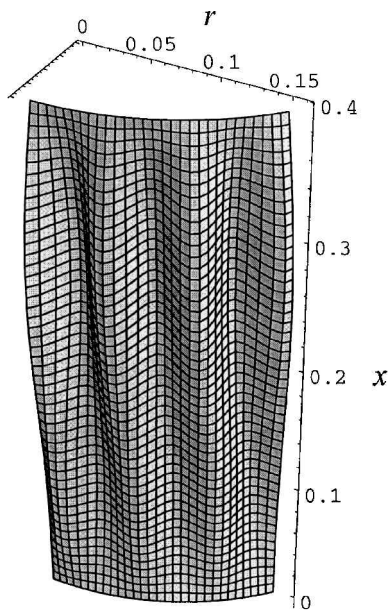

Fig. 8 Mode shape of flutter for $p_\infty = 4500$ Pa in a scale with radial displacement augmented 1000 times. Only a part of 3/23 of the shell circumference is shown.

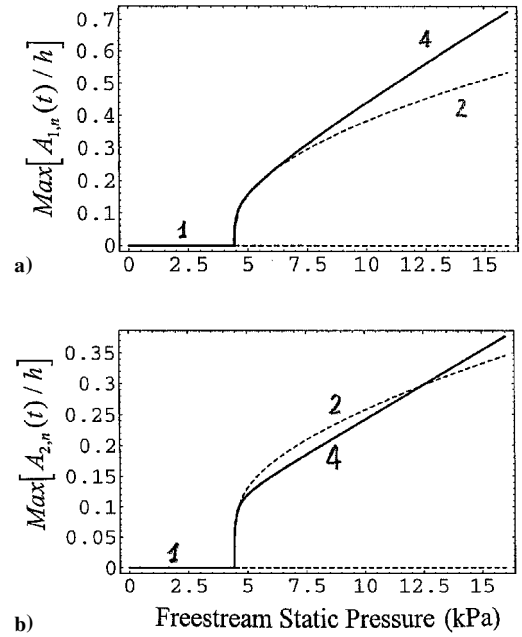

Fig. 9 Amplitude of oscillatory solutions vs the freestream static pressure, for the case of Evensen and Olson: maximum amplitudes of the a) first, $A_{1,n}(t)/h$, and b) second, $A_{2,n}(t)/h$, longitudinal modes. Curve denotation is given in Fig. 4.

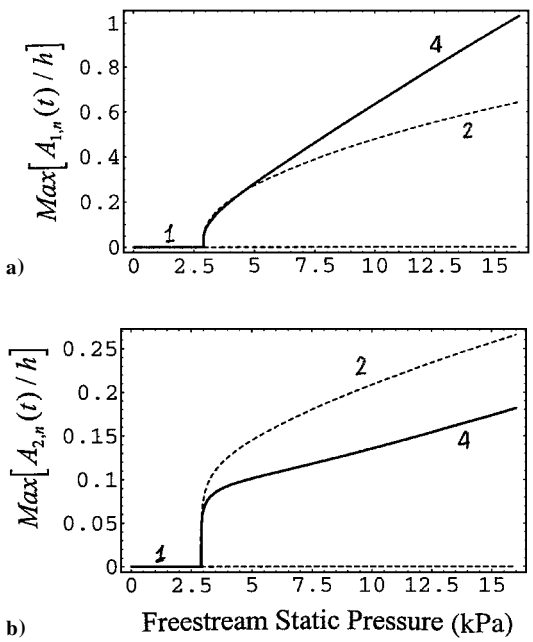

Fig. 10 Amplitude of oscillatory solutions vs the freestream static pressure, for $p_m = 0$: maximum amplitudes of the a) first, $A_{1,n}(t)/h$, and b) second, $A_{2,n}(t)/h$, longitudinal modes. Curve denotation is given in Fig. 4.

the aerodynamic pressure, with $n = 23$ and zero structural damping ($\zeta = 0$). Results are shown in Fig. 9. The onset of instability, already reported in Sec. VII.A, is absolutely coincident with the value in Refs. 12 and 13. However, the behavior of bifurcated branches is different. In particular, the flutter amplitude is of the order of the shell thickness, matching with the experimental results, instead of 10 times this value as found by Evensen and Olson.[12,13] Moreover, no flutter is predicted before the onset of instability predicted by linear theory; also this point agrees with experiments for supersonic flow. (In the case of subsonic flow, subcritical bifurcations occur[3] and are confirmed by experimental results.[1]) Qualitatively, the behavior of the system is the same as discussed for Fig. 4.

The last case investigated is the same as the one presented in Fig. 4, that is, $n = 23$, $\zeta = 0.0005$, and use of Eq. (11) to evaluate the aerodynamic pressure, but with zero differential pressure across the shell skin ($p_m = 0$). The bifurcation diagram is shown in Fig. 10 and is qualitatively similar to those presented in Figs. 4 and 9, confirming the results found for flutter.

Figure 11 shows the softening-type nonlinearity of the shell studied. In fact it gives the frequency-response relationship for the shell of Evensen and Olson[12,13] with $p_m = 0$, $p_\infty = 0$, and $\zeta = 0.0005$. The shell has a modal excitation $f = 0.001\rho h^2 \omega_{1,n}^2 \sin(\pi x/L)\cos(23\theta)\cos(\omega t)$, where $\omega_{1,n}$ is the linear frequency of the mode excited (driven mode) and ω is the excitation frequency. The softening-type nonlinearity is weak. The response has been obtained by using the Auto software[26] and indicates a reduction of $\sim 0.8\%$ of the linear frequency for a vibration amplitude equal to the shell thickness. This result shows that, in the cases studied, the shell loses stability through a supercritical Hopf bifurcation even if the system presents softening-type nonlinearity. In fact, when the freestream static pressure p_∞ is increased from zero to 2890 Pa, that is, just before the onset of flutter, the response of the system to the same excitation is changed into the one given in Fig. 12. A softening-type response is still present for the driven mode, as indicated in Fig. 12a. However, a new hardening-type branch associated with the coupled-mode response, involving the first and second

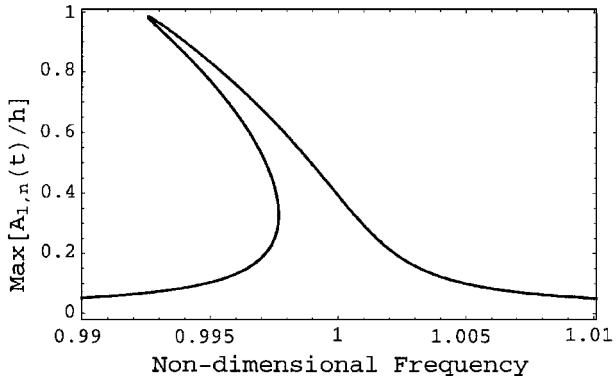

Fig. 11 Forced vibrations of the shell under modal excitation for $p_\infty = 0$, for the case of Evensen and Olson for $p_m = 0$: Nondimensional amplitude of the driven mode vs nondimensional frequency of excitation (frequency of excitation/linear frequency of the driven mode).

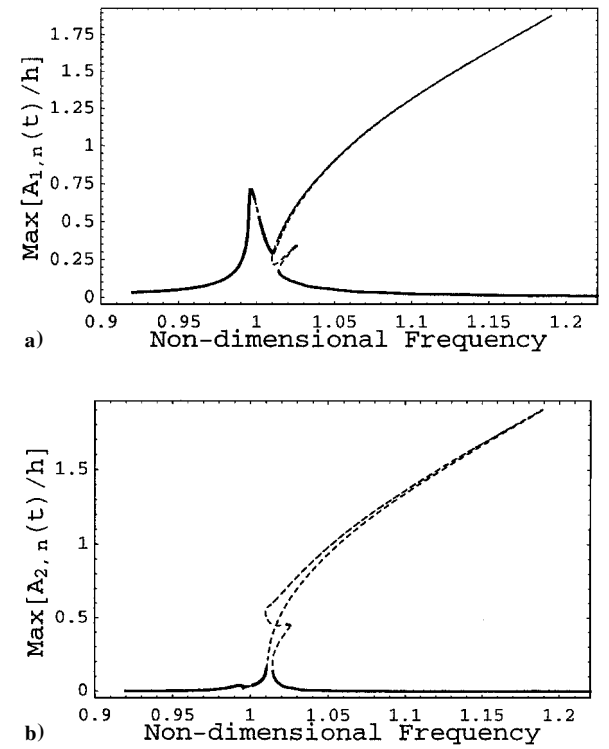

Fig. 12 Forced vibrations of the shell under modal excitation for $p_\infty = 2890$ Pa, for the case of Evensen and Olson for $p_m = 0$: Maximum amplitudes of the a) first, $A_{1,n}(t)/h$ (driven mode), and b) second, $A_{2,n}(t)/h$, longitudinal modes. Curve denotation is given in Fig. 4.

longitudinal modes, appears in Figs. 12a and 12b. This new branch is unstable because the onset of flutter is not yet reached, but it is very close. Figure 12 can be easily related to the hardening flutter response indicated in Fig. 7.

VIII. Conclusions

Numerical results for the shell with small asymmetry show that the instability arises through a standing-wave flutter that loses stability with a very small increment of the freestream static pressure. Then, a traveling-wave flutter appears and remains stable also for a large increment of the freestream static pressure. In case of perfect axial symmetry, all the stable solutions are of the traveling-wave type. In all the studied cases, mild flutter instability has been detected. This is in contrast with violent divergence detected for subsonic flow. No flutter is predicted before the onset of instability predicted by linear theory, and the flutter amplitude is of the order of the shell thickness, which is in very good agreement with the existing experimental data. Traveling-wave flutter presents an almost constant frequency, showing a very small "softening behavior" (caused by the linear reduction of frequency with p_∞) when the curvature-correctionterm is introduced in the piston theory.

The present study is the first one accurately predicting flutter amplitudes of circular cylindrical shells. The present approach could be improved by using more modes in the expansion of the flexural displacement and higher-order piston theory. In particular, the addition of modes with three and four longitudinal half-waves would give a more accurate evaluation of the onset of instability. In contrast, they largely increase the computational effort in the nonlinear study.

Acknowledgment

The authors acknowledge the financial support of the Italian Space Agency.

References

[1]Horn, W., Barr, G. W., Carter, L., and Stearman, R. O., "Recent Contributions to Experiments on Cylindrical Shell Panel Flutter," *AIAA Journal*, Vol. 12, No. 11, 1974, pp. 1481–1490.

[2]Amabili, M., Pellicano, F., and Païdoussis, M. P., "Non-Linear Dynamics and Stability of Circular Cylindrical Shells Containing Flowing Fluid. Part I: Stability," *Journal of Sound and Vibration*, Vol. 225, No. 4, 1999, pp. 655–699.

[3]Amabili, M., Pellicano, F., and Païdoussis, M. P., "Non-Linear Stability of Circular Cylindrical Shells in Annular and Unbounded Axial Flow," *Journal of Applied Mechanics* (submitted for publication).

[4]El Chebair, A., Païdoussis, M. P., and Misra, A. K., "Experimental Study of Annular-Flow-Induced Instabilities of Cylindrical Shells," *Journal of Fluids and Structures*, Vol. 3, 1989, pp. 349–364.

[5]Dowell, E. H., "Flutter of Infinitely Long Plates and Shells. Part II: Cylindrical Shell," *AIAA Journal*, Vol. 4, 1966, pp. 1510–1518.

[6]Olson, M. D., and Fung, Y. C., "Supersonic Flutter of Circular Cylindrical Shells Subjected to Internal Pressure and Axial Compression," *AIAA Journal*, Vol. 4, No. 5, 1966, pp. 858–864.

[7]Olson, M. D., and Fung, Y. C., "Comparing Theory and Experiment for the Supersonic Flutter of Circular Cylindrical Shells," *AIAA Journal*, Vol. 5, No. 10, 1967, pp. 1849–1856.

[8]Barr, G. W., and Stearman, R. O., "Influence of a Supersonic Flowfield on the Elastic Stability of Cylindrical Shells," *AIAA Journal*, Vol. 8, No. 6, 1970, pp. 993–1000.

[9]Ganapathi, M., Varadan, T. K., and Jijen, J., "Field-Consistent Element Applied to Flutter Analysis of Circular Cylindrical Shells," *Journal of Sound and Vibration*, Vol. 171, No. 4, 1994, pp. 509–527.

[10]Librescu, L., "Aeroelastic Stability of Orthotropic Heterogeneous Thin Panels in the Vicinity of the Flutter Critical Boundary. Part I: Simply Supported Panels," *Journal de Mécanique*, Vol. 4, No. 1, 1965, pp. 51–76.

[11]Librescu, L., "Aeroelastic Stability of Orthotropic Heterogeneous Thin Panels in the Vicinity of the Flutter Critical Boundary. Part II." *Journal de Mécanique*, Vol. 6, No. 1, 1967, pp. 133–152.

[12]Evensen, D. A., and Olson, M. D., "Nonlinear Flutter of a Circular Cylindrical Shell in Supersonic Flow," NASA TN D-4265, 1967.

[13]Evensen, D. A., and Olson, M. D., "Circumferentially Travelling Wave Flutter of a Circular Cylindrical Shell," *AIAA Journal*, Vol. 6, No. 8, 1968, pp. 1522–1527.

[14]Evensen, D. A., "Nonlinear Flexural Vibrations of Thin-Walled Circular Cylinders," NASA TN D-4090, 1967.

[15]Ginsberg, J. H., "Large Amplitude Forced Vibrations of Simply Supported Thin Cylindrical Shells," *Journal of Applied Mechanics*, Vol. 40, No. 2, 1973, pp. 471–477.

[16]Chen, J. C., and Babcock, C. D., "Nonlinear Vibration of Cylindrical Shells," *AIAA Journal*, Vol. 13, No. 7, 1975, pp. 868–876.

[17]Amabili, M., Pellicano, F., and Païdoussis, M. P., "Nonlinear Vibrations of Simply Supported, Circular Cylindrical Shells, Coupled to Quiescent Fluid," *Journal of Fluids and Structures*, Vol. 12, No. 7, 1998, pp. 883–918.

[18]Amabili, M., Pellicano, F., and Païdoussis, M. P., "Non-Linear Dynamics and Stability of Circular Cylindrical Shells Containing Flowing Fluid, Part II: Large Amplitude Vibrations Without Flow," *Journal of Sound and Vibration*, Vol. 228, No. 5, 1999, pp. 1103–1124.

[19]Olsson, U., "Supersonic Flutter of Heated Circular Cylindrical Shells with Temperature-Dependent Material Properties," *AIAA Journal*, Vol. 16, No. 4, 1978, pp. 360–362.

[20]Gonçalves, P. B., and Batista, R. C., "Non-Linear Vibration Analysis of Fluid-Filled Cylindrical Shells," *Journal of Sound and Vibration*, Vol. 127, No. 1, 1988, pp. 133–143.

[21] Dowell, E. H., and Ventres, C. S., "Modal Equations for the Nonlinear Flexural Vibrations of a Cylindrical Shell," *International Journal of Solids and Structures*, Vol. 4, 1968, pp. 975–991.

[22] Atluri, S., "A Perturbation Analysis of Non-Linear Free Flexural Vibrations of a Circular Cylindrical Shell," *International Journal of Solids and Structures*, Vol. 8, 1972, pp. 549–569.

[23] Amabili, M., Pellicano, F., and Païdoussis, M. P., "Non-Linear Dynamics and Stability of Circular Cylindrical Shells Containing Flowing Fluid, Part III: Truncation Effect Without Flow and Experiments," *Journal of Sound and Vibration* (to be published).

[24] Wolfram, S., *The Mathematica Book*, 4th ed., Cambridge Univ. Press, Cambridge, England, U.K., 1999.

[25] Yamaki, N., *Elastic Stability of Circular Cylindrical Shells*, North-Holland, Amsterdam, 1984.

[26] Doedel, E. J., Champneys, A. R., Fairgrieve, T. F., Kuznetsov, Y. A., Sandstede, B., and Wang, X., "AUTO 97: Continuation and Bifurcation Software for Ordinary Differential Equations (with HomCont)," Concordia Univ., Montreal, QC, Canada, 1998.

A. N. Palazotto
Associate Editor